# Enhancing the $CO_2$ Adsorption Performance of UiO-66 by Imidazolium-Based Room-Temperature Ionic Liquids (RTILs) Incorporation

**Laela Mukaromah, Andi Haryanto, Yessi Permana, and Aep Patah***

*Division of Inorganic and Physical Chemistry, Faculty of Mathematics and Natural Sciences, Institut Teknologi Bandung, Jl. Ganesha No. 10, Bandung 40132, Indonesia*

** **Corresponding author:***

*email: aep@itb.ac.id*

*Received: May 23, 2023*
*Accepted: July 17, 2023*

**DOI:** 10.22146/ijc.84669

***Abstract:*** *Functionalization of metal-organic frameworks resulting in efficient $CO_2$ adsorption materials became substantial in preventing the worsening environment upon the emission of $CO_2$. In this study, several room-temperature ionic liquids (RTILs) with an imidazolium-based cation of 1-butyl-3-methylimidazolium $[bmim]^+$ and anions of bis(trifluoromethylsulfonyl)imide $[TFSI]^-$, trifluoromethanesulfonate $[OTf]^-$, hexafluorophosphate $[PF_6]^-$, and tetrafluoroborate $[BF_4]^-$ were incorporated into UiO-66 by wet impregnation method under air. The RTILs/UiO-66 composites were characterized by PXRD, FTIR, TGA, nitrogen physisorption, and $CO_2$ adsorption. Based on the type of anions of imidazolium-based RTILs, the $CO_2$ uptake of RTILs/UiO-66 composites followed the trend: $[OTf]^- > [TFSI]^- > [PF_6]^- > [BF_4]^-$ at low temperature (273 K) and pressure (100 kPa). The $CO_2$ uptake of pristine UiO-66 increased approximately 1.5 times upon incorporating [bmim][OTf]. The type of anions of imidazolium-based RTILs influences the $CO_2$ adsorption performance of RTILs/UiO-66 composites in which anions containing fluoroalkyl group ($[OTf]^-$, $[TFSI]^-$) exhibited a higher $CO_2$ uptake compared to inorganic fluorinated anions ($[BF_4]^-$, $[PF_6]^-$). Hence, the incorporation of hydrophobic imidazolium-based RTILs showed a potential to enhance the performance of UiO-66 for $CO_2$ adsorption application.*

***Keywords:*** *$CO_2$ adsorption; imidazolium-based RTILs; incorporation; UiO-66*

## ■ INTRODUCTION

High greenhouse gas (GHG) emissions directly induce global warming and climate change. They are serious environmental issues that have been attracting worldwide attention [1]. Carbon dioxide ($CO_2$), the major component in GHG emissions, is mostly generated from combustion sources [2]. The amount of $CO_2$ released to the atmosphere significantly increases following the rapid development in industrial and energy infrastructures with a high demand for fossil fuels [3]. To prevent the worsening impact, the utilization of natural gas producing less $CO_2$ emission over fossil fuels and coal has been initiated [4]. Natural gas offers several advantages, such as being more abundant, environmentally friendly, and relatively inexpensive [5]. However, raw natural gas also contains impurities like $CO_2$, which must be removed before further use due to its corrosive property [6].

Natural gas purification from $CO_2$ has been extensively conducted using a robust technology known as amine scrubbing [7]. This technology generally uses a primary alkanolamine solution of 20–30 wt.% monoethanolamine, besides diethanolamine, triethanolamine, or *N*-methyldiethanolamine, as secondary, tertiary, and ternary alkanolamines, respectively [8]. Although this technology is highly efficient for $CO_2$ separation, alkanolamine solutions also have several drawbacks, *i.e.*, amine degradation toward heating, high energy demand for amine regeneration, and corrosive toward equipment, leading to environmental issues and significant expense for industrial scale [9]. Therefore, a thermally stable material needs to be developed as an alternative approach for $CO_2$ separation on a large scale.

An emerging generation of crystalline materials with

exceptional porosity is defined as metal-organic frameworks (MOFs), also known as porous coordination polymers [10]. The structure of MOFs is built from metal ions in the form of secondary building units as nodes and organic linkers as spokes, connected with coordination bonds [11]. MOFs are recognized for their tunability and feasibility in structure, which make them ideal for gas adsorption and separation [12]. Nevertheless, designing MOFs with excellent $CO_2$ selectivity similar to alkanolamine solutions remains challenging [13]. Several post-synthetic modifications on MOFs are carried out to enhance the $CO_2$ selectivity. Despite its high $CO_2$ capture, the functionalization of MOFs using alkylamines deals with pore accessibility control upon the formation of amine aggregates [14]. The incorporation of MOFs into polymer membranes concerns with non-uniform particle distribution within the matrix, which can cause severe agglomeration [15].

A novel functionalization of MOFs with room-temperature ionic liquids (RTILs) has been increasingly investigated, particularly using imidazolium-based cation. RTILs are liquid-phase salts at room temperature or lower, commonly arranged from asymmetric organic cations with symmetric organic or inorganic anions [16]. Owing several outstanding properties, *i.e.*, high thermal stability, null volatility, negligible flammability, and good solubility toward $CO_2$ make them promising to be incorporated into MOFs for $CO_2$ adsorption or separation [17]. Zeeshan et al. [13] investigated the performance of [hemim][DCA]/ZIF-8 composite in a core-shell type for $CO_2$ separation. They concluded that the composite exhibits $CO_2$ adsorption and $CO_2/CH_4$ selectivity up to 5.7 and 45 times higher, respectively, compared to the unmodified ZIF-8 at low pressure. Kinik et al. [18] examined the incorporation of ZIF-8 with [bmim][$PF_6$] for $CO_2$ separation. They found that the double $CO_2$ selectivity over $CH_4$ and $N_2$ is generated from ZIF-8 and [bmim][$PF_6$] direct interaction. Oliveira et al. [19] performed the molecular simulations of [bmim][$PF_6$] and [bmim][TFSI] incorporated with MIL-100(Fe) for $CO_2$ adsorption. They showed that the presence of RTILs increases $CO_2$ adsorption and selectivity ($CO_2/CH_4$ and $CO_2/N_2$) at low pressure.

Herein, we study the incorporation of imidazolium-based RTILs into Zr-based MOFs of UiO-66 for $CO_2$ adsorption. Featuring $Zr_6O_4(OH)_4$ nodes in 12 coordination of linkers [20], UiO-66 shows excellent thermal stability alongside octahedral and tetrahedral cages that make it suitable for gas adsorption or separation [21]. While imidazolium-based RTILs are widely utilized for $CO_2$ adsorption or separation owing to their good $CO_2$ solubility [22]. Furthermore, the influence of the following anions: tetrafluoroborate $[BF_4]^-$, hexafluorophosphate $[PF_6]^-$, trifluoromethanesulfonate $[OTf]^-$, and bis(trifluoromethylsulfonyl)imide $[TFSI]^-$, with a cation of 1-butyl-3-methylimidazolium $[bmim]^+$ in the imidazolium-based RTILs/UiO-66 composites is investigated toward the $CO_2$ adsorption performance at low temperature and pressure.

## ■ EXPERIMENTAL SECTION

### Materials

All materials were commercially available and employed without further purification: 1-butyl-3-methylimidazolium tetrafluoroborate ([bmim][$BF_4$], ≥98% purity Merck, Germany), 1-butyl-3-methylimidazolium hexafluorophosphate ([bmim][$PF_6$], 97% purity Merck, Germany), 1-butyl-3-methylimidazolium trifluoromethanesulfonate ([bmim][OTf], 97% purity Merck, Germany), 1-butyl-3-methylimidazolium bis(trifluoromethylsulfonyl)imide ([bmim][TFSI], ≥98% purity Merck, Germany), zirconium(IV) chloride ($ZrCl_4$, ≥98% purity Merck, Germany), 1,4-benzenedicarboxylic acid ($H_2BDC$, ≥98% purity Merck, Germany), *N*,*N*-dimethylformamide (DMF, ≥99.8% purity Merck, Germany), chloroform (≥99% purity Merck, Germany), and acetone (≥99.8% purity Merck, Germany).

### Instrumentation

Phase identification of samples was collected by powder X-ray diffractometer (PXRD, Rigaku MiniFlex 600) in the range of 2θ from 5 to 50° using a source of radiation of Cu-Kα and wavelength of 1.540593 Å. The functional group coordination of samples was obtained by Fourier-transformed infrared spectrometer (FTIR,

Bruker Alpha series) with a splitter of ZnSe beam in the wavenumber range from 500 to 4000 $cm^{-1}$ using KBr to disperse the samples. The thermal stability of samples was performed on a thermogravimetric analysis instrument (TGA, Hitachi STA7300) by heating the samples on an aluminium pan in the range of temperature from 30 to 500 °C with 20 °C $cm^{-1}$ heating rate under nitrogen. Sample pore analysis was carried out using a nitrogen physisorption measurements instrument at 77 K (Quantachrome NOVA 2200e). $CO_2$ adsorption performance of samples was conducted using $CO_2$ adsorption measurements instrument at 273 K (MicrotracBel BELSORP-max). Before nitrogen physisorption and $CO_2$ adsorption measurements, UiO-66 and RTILs/UiO-66 composites samples were degassed at 160 and 105 °C for 6 h under a vacuum, respectively.

### Procedure

#### *Synthesis of UiO-66*

UiO-66 was synthesized using a conventional heating method, slightly modified from the previous reports [20,23]. As much as 0.233 g of $ZrCl_4$ (1.0 mmol) was mixed with 10 mL of DMF in a nitrogen-charged glove box and then sonicated for 10 min at room temperature. An amount of 0.166 g of 1,4-benzenedicarboxylic acid ($H_2BDC$, 1.0 mmol) and 0.1 mL of acetic acid 10% (v/v) were added to the mixture, and then sonicated again for 20 min. The mixture was put into the oven and heated at 120 °C for 1 d. The reaction solvent was decanted from the solid product after cooling down. The washing process was conducted by soaking the solid product in 5 mL of chloroform, decanted, and repeated three times. After that, the solid product was filtered at room temperature and then degassed at 160 °C for 6 h under a vacuum.

#### *Synthesis of RTILs/UiO-66 composites*

Imidazolium-based RTILs/UiO-66 composites with 30% loading of RTILs were synthesized using the wet impregnation method, slightly modified from the previous report [24]. The first composite was prepared by room temperature stirring of 15 mL of acetone and 0.15 g of [bmim][$BF_4$] for 1 h under air. The mixture was added with 0.35 g of activated UiO-66, and then continuously stirred for 6 h. The solid product was filtered at room temperature, and then degassed at 105 °C for 6 h under a vacuum. Other imidazolium-based RTILs/UiO-66 composites with [bmim][$PF_6$], [bmim][OTf], and [bmim][TFSI] were also synthesized according to this procedure.

## ■ RESULTS AND DISCUSSION

The incorporation of imidazolium-based RTILs series, *i.e.*, [bmim][$BF_4$], [bmim][$PF_6$], [bmim][OTf], and [bmim][TFSI] denoted as Im-B, Im-P, Im-O, and Im-T, respectively, into zirconium-based MOFs of UiO-66 was carried out by wet impregnation method at room temperature under air. The four RTILs/UiO-66 composites hereafter were denoted as Im-B/UiO-66, Im-P/UiO-66, Im-O/UiO-66, and Im-T/UiO-66. Solvated RTILs/UiO-66 composites show consistency with the characteristic diffraction peaks of pristine UiO-66 at 2θ of 7.43 and 8.55° corresponding to reflection planes of (111) and (200), respectively, in agreement with the previous studies [25-26], as presented in the PXRD patterns (Fig. 1). Furthermore, there is no decrease in the relative intensity of UiO-66 in comparison to Im-B/UiO-66, Im-P/UiO-66, Im-O/UiO-66, and Im-T/UiO-66 composites explain that the incorporation of imidazolium-based RTILs into UiO-66 does not alter its pristine structure, following previous reports on [bmim][$BF_4$]/CuBTC and [bmim][$PF_6$]/ZIF-8 composites [18,24]. PXRD patterns of all RTILs/UiO-66 composites also remain consistent after degassing (Fig. 2).

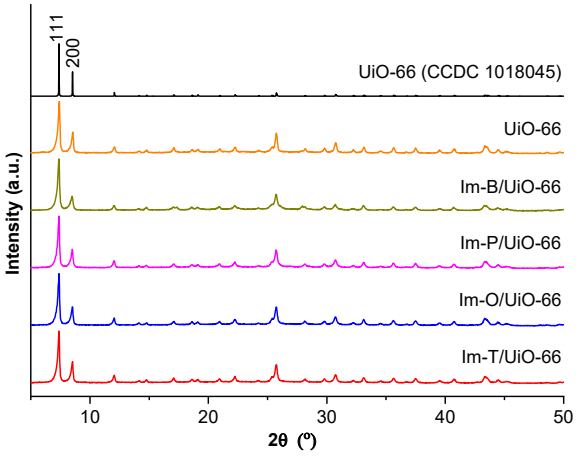


**Fig 1.** PXRD patterns of UiO-66 (orange), Im-B/UiO-66 (dark yellow), Im-P/UiO-66 (magenta), Im-O/UiO-66 (blue), and Im-T/UiO-66 (red)

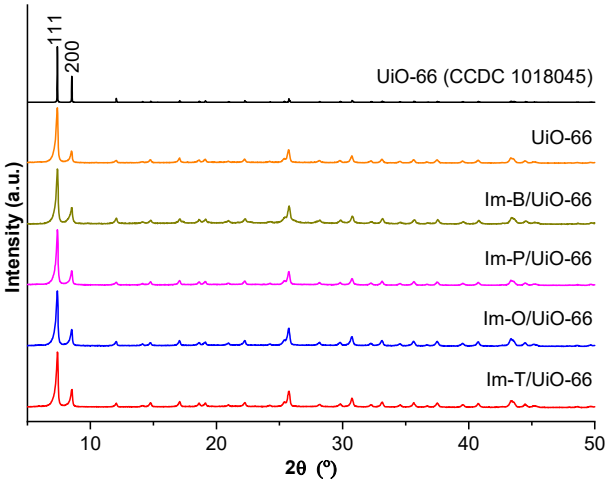


**Fig 2.** PXRD patterns of activated UiO-66 (orange), Im-B/UiO-66 (dark yellow), Im-P/UiO-66 (magenta), Im-O/UiO-66 (blue), and Im-T/UiO-66 (red)

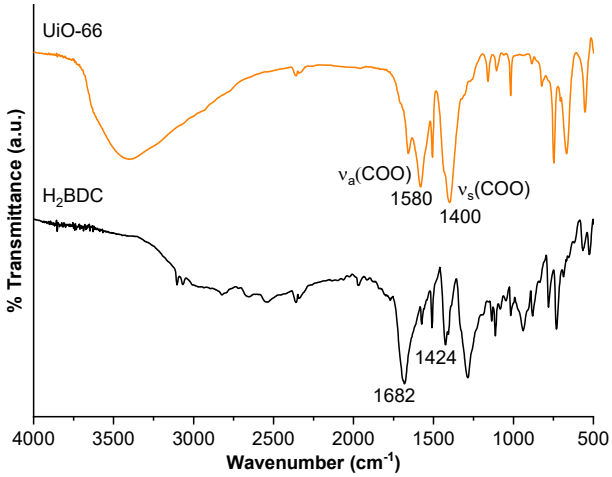


**Fig 3.** FTIR spectra of UiO-66 (orange) and $H_2BDC$ ligand (black)

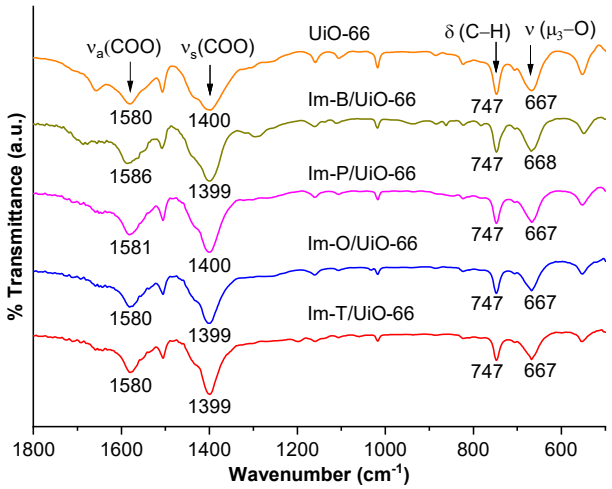


**Fig 4.** FTIR spectra of UiO-66 (orange), Im-B/UiO-66 (dark yellow), Im-P/UiO-66 (magenta), Im-O/UiO-66 (blue), and Im-T/UiO-66 (red)

Fig. 3 displays the FTIR spectra of pristine UiO-66 and $H_2BDC$ ligand. The peaks at 1682 and 1424 $cm^{-1}$ correspond to asymmetric and symmetric stretching bands of the carboxyl group of $H_2BDC$. The formation of $Zr_6O_4(OH)_4(CO_2)_{12}$ clusters of UiO-66 is confirmed by the weakening of carboxyl groups vibrations of $H_2BDC$, from 1682 and 1424 $cm^{-1}$ in the free ligand to 1580 and 1400 $cm^{-1}$ in the UiO-66, in agreement with the previous study [25]. However, the significant changes in the peak positions of UiO-66 upon the incorporation with imidazolium-based RTILs were hardly observed from the FTIR spectra from 500 to 1800 $cm^{-1}$ range of wavenumber (Fig. 4). There is no shifting from the $\mu_3$–O bridging bond peak of UiO-66 at 667 $cm^{-1}$ explaining the direct interactions between imidazolium-based RTILs and metal nodes of UiO-66 in the Im-B/UiO-66, Im-P/UiO-66, Im-O/UiO-66, and Im-T/UiO-6 composites were not strong, similar to reported [bmim][$MeSO_4$]/UiO-66 composite [25]. Furthermore, the stretching vibrations of the carboxyl group and bending vibration of –CH of UiO-66 also remain the same after incorporation, confirming the lack of interactions with RTILs. In this case, water as impurities in RTILs and unremoved synthesis solvents inside the pore of MOFs likely contribute to the weak interactions between the two components [13,16].

Thermogravimetric analysis (TGA) curves of Im-B/UiO-66, Im-P/UiO-66, Im-O/UiO-66, and Im-T/UiO-66 composites demonstrate a more extensive weight loss than pristine UiO-66 upon heating to 500 °C under nitrogen (Fig. 5). Im-O/UiO-66 and Im-T/UiO-66 composites generate an identical decomposition temperature, followed by the Im-P/UiO-66 composite, which is similar, but the Im-B/UiO-66 composite exhibits a different trend. This result may also be influenced by the hydrophilicity property of the imidazolium-based RTILs, in which [bmim][OTf], [bmim][TFSI], and [bmim][$PF_6$] are hydrophobic, while [bmim][$BF_4$] is hydrophilic [27]. The first weight loss of about 13.6, 23, 24.5, and 24.3% are observed below 100 °C, corresponding

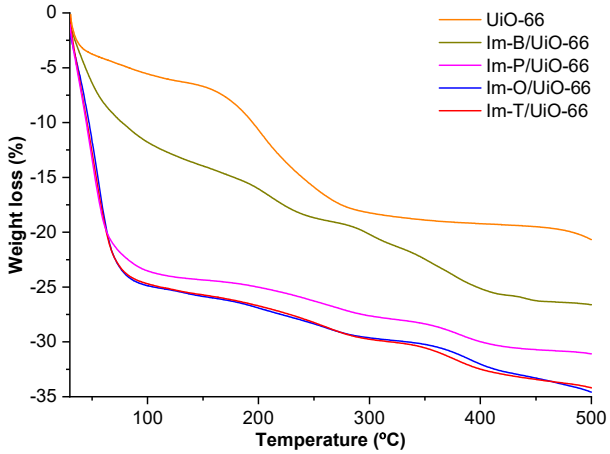


**Fig 5.** TGA curves of UiO-66 (orange), Im-B/UiO-66 (dark yellow), Im-P/UiO-66 (magenta), Im-O/UiO-66 (blue), and Im-T/UiO-66 (red)

on the removal of acetone molecules (RTILs impregnation solvent) for Im-B/UiO-66, Im-P/UiO-66, Im-O/UiO-66, and Im-T/UiO-66 composites, respectively. At the same temperature, the Im-B/UiO-66 composite shows less acetone removal, indicating the composite is more polar than other RTILs/UiO-66 composites. The second weight loss from 100 to 300 °C is ascribed to the removal of moisture and DMF molecules (UiO-66 synthesis solvent). Meanwhile, the Im-B/UiO-66 composite shows two weight loss steps up to 300 °C. The weight loss from 300 to 400 °C corresponds to the decomposition of [bmim][$BF_4$], [bmim][$PF_6$], [bmim][OTf], and [bmim][TFSI] from the RTILs/UiO-66 composites. Furthermore, the frameworks of UiO-66 start to collapse above 450 °C for pristine MOFs, above 400 °C for the Im-B/UiO-66 composite, and for other composites above 350 °C, referring to the partial loss of BDC linkers. Accordingly, incorporating several imidazolium-based RTILs into UiO-66 alleviates the pristine thermal stability, illustrating the interaction of both components in the composites, consistent with previous studies [24,28].

Nitrogen physisorption measurements at 77 K reveal type I adsorption isotherm, indicating that pristine UiO-66 and all RTILs/UiO-66 composites are microporous materials (Fig. 6). The difference in hydrophilicity property of imidazolium-based RTILs likely influences the nitrogen uptake of the RTILs/UiO-66 composites. Im-B/UiO-66, Im-P/UiO-66, Im-O/UiO-66, and Im-T/UiO-66 composites exhibit nitrogen uptake of 285.62, 412.44, 429.69, and 437.50 $cm^3\ g^{-1}$, respectively, while for pristine UiO-66 is 350.87 $cm^3\ g^{-1}$. The Im-B/UiO-66 composite with hydrophilic RTILs shows a decrement in pore analysis values compared to pristine UiO-66, while Im-P/UiO-66, Im-O/UiO-66, and Im-T/UiO-66 composites with hydrophobic RTILs possess larger values (Table 1). This result trend is the opposite of several previous studies, in which incorporating RTILs reduces pore analysis values of pristine MOFs even though both components have similar hydrophilicity [19,24]. The incomplete removal of trapped DMF molecules from the frameworks of UiO-66 during degassing process may limit the accessibility of

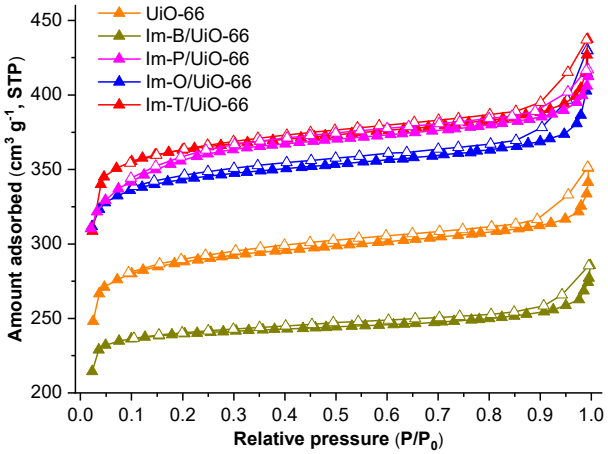


**Fig 6.** $N_2$ physisorption isotherms of UiO-66 (orange), Im-B/UiO-66 (dark yellow), Im-P/UiO-66 (magenta), Im-O/UiO-66 (blue), and Im-T/UiO-66 (red)

**Table 1.** Pore analysis of UiO-66 and RTILs/UiO-66 composites

| Sample | BET surface area ($m^2\ g^{-1}$) | Total pore volume ($cm^3\ g^{-1}$) |
|---|---|---|
| UiO-66 | 883 | 0.543 |
| Im-B/UiO-66 | 722 | 0.442 |
| Im-P/UiO-66 | 1100 | 0.645 |
| Im-O/UiO-66 | 1043 | 0.665 |
| Im-T/UiO-66 | 1104 | 0.677 |

nitrogen due to pore blockage, which generates MOFs with a low Brunauer-Emmett-Teller (BET) surface area [29]. Conversely, the enhanced BET surface area observed in the Im-P/UiO-66, Im-O/UiO-66, and Im-T/UiO-66 composites can be assigned to the additional role of acetone as the exchange solvent for DMF from the structure of UiO-66, aside as the impregnation solvent for RTILs. Therefore, instead of prolonging the degassing process of MOFs using the thermal activation method, employing acetone for the washing process of MOFs can be an alternative way to optimize the pore analysis values and minimize the structural damage of MOFs [30].

$CO_2$ adsorption performances of pristine UiO-66, Im-B/UiO-66, Im-P/UiO-66, Im-O/UiO-66, and Im-T/UiO-66 composites measured at 273 K exhibit a similar result trend as observed in TGA measurements, with only Im-B/UiO-66 composite displaying an opposite behavior compared to other composites. Incorporating imidazolium-based RTILs enhances $CO_2$ uptake of UiO-66 in the RTILs/UiO-66 composites as presented in the $CO_2$ adsorption isotherms (Fig. 7). The $CO_2$ uptake amounts of Im-B/UiO-66, Im-P/UiO-66, Im-O/UiO-66, and Im-T/UiO-66 composites are 28.016, 67.647, 75.965, and 72.300 $cm^3\ g^{-1}$, respectively, while pristine UiO-66 is 51.382 $cm^3\ g^{-1}$. Although some previous simulation and experimental studies reported the improvement in $CO_2$ uptake of MOFs upon the incorporation of RTILs at low pressure, such as in RTILs/ZIF-8 [13,18], RTILs/MIL-100(Fe) [19], and RTILs/CuBTC composites [31], the reduced $CO_2$ uptake was declared in RTILs/UiO-66 and RTILs/NU-1000 composites [32]. The shrinkage in BET surface area of UiO-66 upon the incorporation of [bmim][$BF_4$] from 883 to 722 $m^2\ g^{-1}$ yields a less number of adsorption sites in the Im-B/UiO-66 composite leading to a low $CO_2$ uptake, similar to a previous report on [bmim][$BF_4$]/CuBTC composite [24]. In addition, a low $CO_2$ uptake in Im-B/UiO-66 composite is presumably influenced by the difference in polarity from $[BF_4]^-$ anion compared to other anions, making it less preferable for a polar gas like $CO_2$ [28], following TGA measurement results.

Nevertheless, the pore analysis values of the four imidazolium-based RTILs/UiO-66 composites are not the main factor determining their $CO_2$ uptake when the $CO_2$ adsorption performances are measured at low pressure. For instance, the Im-T/UiO-66 composite possesses the largest BET surface area, yet the highest $CO_2$ uptake is found in the Im-O/UiO-66 composite. Aside from the BET surface area, the solubility of $CO_2$ in RTILs also holds a prominent role in $CO_2$ uptake. Aki et al. [33] found that the type of anion in imidazolium-based RTILs strongly influences the $CO_2$ solubility, in which anions containing fluoroalkyl group ($[TFSI]^-$, $[OTf]^-$) generated a higher $CO_2$ uptake compared to inorganic fluorinated anions ($[PF_6]^-$, $[BF_4]^-$). Muldoon et al. [34] revealed that the solubility of $CO_2$ was improved following the increase of fluoroalkyl chains in either cation or anion of RTILs. Even though $[TFSI]^-$ anion contains more fluoroalkyl group than $[OTf]^-$ anion, the Im-T/UiO-66 composite exhibits a lower $CO_2$ uptake compared to the Im-O/UiO-66 composite, which is likely

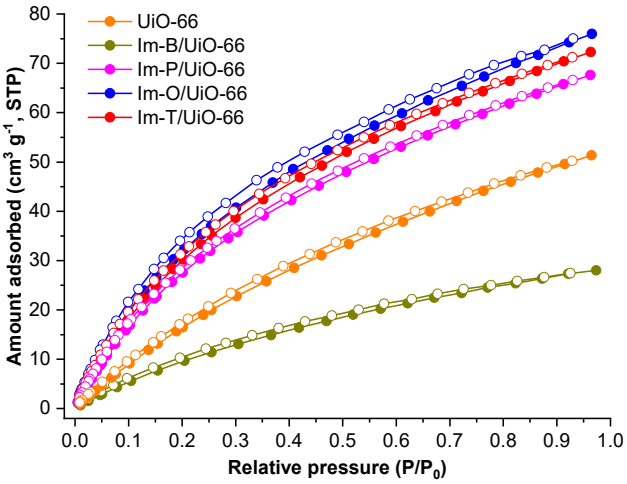


**Fig 7.** $CO_2$ adsorption isotherms of UiO-66 (orange), Im-B/UiO-66 (dark yellow), Im-P/UiO-66 (magenta), Im-O/UiO-66 (blue), and Im-T/UiO-66 (red)

**Table 2.** Cation and anion radii of imidazolium-based RTILs obtained from reference [35]

| Ion | Ionic radius (Å) |
|---|---|
| $[bmim]^+$ | 4.57 |
| $[BF_4]^-$ | 3.37 |
| $[PF_6]^-$ | 3.58 |
| $[OTf]^-$ | 3.89 |
| $[TFSI]^-$ | 4.44 |

attributed to the larger ionic radius of $[TFSI]^-$ than $[OTf]^-$, as presented in Table 2. Therefore, aside from the increased fluorination number of the anion, the size of anion may also influence the solubility of $CO_2$ resulting in the $CO_2$ uptake order of Im-O/UiO-66 > Im-T/UiO-66 > Im-P/UiO-66 > Im-B/UiO-66.

## ■ CONCLUSION

Imidazolium-based RTILs/UiO-66 composites with 30% loading of RTILs, *i.e.*, [bmim][$BF_4$]/UiO-66, [bmim][$PF_6$]/UiO-66, [bmim][OTf]/UiO-66, and [bmim][TFSI]/UiO-66 were successfully synthesized by wet impregnation method under air. The enhanced $CO_2$ uptake measured at low pressure (100 kPa) was observed upon the incorporation of [bmim][$PF_6$], [bmim][OTf], and [bmim][TFSI] into UiO-66, while [bmim][$BF_4$] showed the reduced $CO_2$ uptake compared to pristine UiO-66. The BET surface area of [bmim][$BF_4$]/UiO-66, [bmim][$PF_6$]/UiO-66, [bmim][OTf]/UiO-66, and [bmim][TFSI]/UiO-66 composites was 722, 1100, 1043, and 1104 $m^2\ g^{-1}$, respectively. However, the $CO_2$ uptake amounts of [bmim][$BF_4$]/UiO-66, [bmim][$PF_6$]/UiO-66, [bmim][OTf]/UiO-66, and [bmim][TFSI]/UiO-66 composites were 28.016, 67.647, 75.965, and 72.300 $cm^3\ g^{-1}$, respectively. These results explained that besides the BET surface area, the properties of the anion of RTILs, such as fluorination number, polarity, and ionic radii, might also influence the $CO_2$ adsorption performance of imidazolium-based RTILs/UiO-66 composites at low pressure, following the order: [bmim][OTf]/UiO-66 > [bmim][TFSI]/UiO-66 > [bmim][$PF_6$]/UiO-66 > [bmim][$BF_4$]/UiO-66. Furthermore, the $CO_2$ adsorption performances at different temperatures and reusability of these imidazolium-based RTILs/UiO-66 composites must be investigated for future application.

## ■ ACKNOWLEDGMENTS

This study was funded by Institut Teknologi Bandung (ITB) through the Research Program 2020 (2I/I1.C01/PL/2020). The authors thank Prof. Satoshi Horike and Dr. Masakazu Higuchi for the $CO_2$ adsorption measurements at the Institute for Integrated Cell-Material Sciences (iCeMS), Kyoto University Institute for Advanced Study (KUIAS), Japan.

## ■ AUTHOR CONTRIBUTIONS

Conceptualization: Laela Mukaromah and Andi Haryanto, methodology: Laela Mukaromah and Andi Haryanto, data acquisition: Laela Mukaromah and Andi Haryanto, data analysis: Laela Mukaromah, Andi Haryanto, and Aep Patah, funding acquisition: Aep Patah and Yessi Permana, resources: Aep Patah and Yessi Permana, writing-original draft: Laela Mukaromah, writing-review and editing: Laela Mukaromah, Andi Haryanto, and Aep Patah. All authors have agreed to the final version of this manuscript.

## ■ REFERENCES

[1] Sylvia, N., Fitriani, F., Dewi, R., Mulyawan, R., Muslim, A., Husin, H., Yunardi, Y., and Reza, M., 2021, Characterization of bottom ash waste adsorbent from palm oil plant boiler burning process to adsorb carbon dioxide in a fixed bed column, *Indones. J. Chem.*, 21 (6), 1454–1462.

[2] Wardani, A.R.K., and Widiastuti, N., 2016, Synthesis of zeolite-X supported on glasswool for $CO_2$ capture material: Variation of immersion time and NaOH concentration at glasswool activation, *Indones. J. Chem.*, 16 (1), 1–7.

[3] Li, B., Wen, H.M., Yu, Y., Cui, Y., Zhou, W., Chen, B., and Qian, G., 2018, Nanospace within metal-organic frameworks for gas storage and separation, *Mater. Today Nano*, 2, 21–49.

[4] Chen, Y., Wu, H., Liu, Z., Sun, X., Xia, Q., and Li, Z., 2018, Liquid-assisted mechanochemical synthesis of copper based MOF-505 for the separation of $CO_2$ over $CH_4$ or $N_2$, *Ind. Eng. Chem. Res.*, 57 (2), 703–709.

[5] Belmabkhout, Y., Bhatt, P.M., Adil, K., Pillai, R.S., Cadiau, A., Shkurenko, A., Maurin, G., Gongping, L., Koros, W.J., and Eddaoudi, M., 2018, Natural gas upgrading using a fluorinated MOF with tuned $H_2S$ and $CO_2$ adsorption selectivity, *Nat. Energy*, 3 (12), 1059–1066.

[6] Sun, T., Ren, X., Hu, J., and Wang, S., 2014, Expanding pore size of Al-BDC metal-organic frameworks as a way to achieve high adsorption

selectivity for $CO_2/CH_4$ separation, *J. Phys. Chem. C*, 118 (29), 15630–15639.

[7] Gao, W., Zheng, W., Sun, W., and Zhao, L., 2022, Understanding the effective capture of $H_2S/CO_2$ from natural gas using ionic liquid@MOF composites, *J. Phys. Chem. C*, 126 (46), 19872–19882.

[8] Sumida, K., Rogow, D.L., Mason, J.A., McDonald, T.M., Bloch, E.D., Herm, Z.R., Bae, T.H., and Long, J.R., 2012, Carbon dioxide capture in metal-organic frameworks, *Chem. Rev.*, 112 (2), 724–781.

[9] Yoon, H.C., Rallapalli, P.B.S., Beum, H.T., Han, S.S., and Kim, J.N., 2018, Hybrid postsynthetic functionalization of tetraethylenepentamine onto MIL-101(Cr) for separation of $CO_2$ from $CH_4$, *Energy Fuels*, 32 (2), 1365–1373.

[10] Kitao, T., Zhang, Y., Kitagawa, S., Wang, B., and Uemura, T., 2017, Hybridization of MOFs and polymers, *Chem. Soc. Rev.*, 46 (11), 3108–3133.

[11] Furukawa, S., Reboul, J., Diring, S., Sumida, K., and Kitagawa, S., 2014, Structuring of metal-organic frameworks at the mesoscopic/macroscopic scale, *Chem. Soc. Rev.*, 43 (16), 5700–5734.

[12] Li, H., Wang, K., Sun, Y., Lollar, C.T., Li, J., and Zhou, H.C., 2018, Recent advances in gas storage and separation using metal–organic frameworks, *Mater. Today*, 21 (2), 108–121.

[13] Zeeshan, M., Nozari, V., Yagci, M.B., Isik, T., Unal, U., Ortalan, V., Keskin, S., and Uzun, A., 2018, Core-shell type ionic liquid/metal organic framework composite: An exceptionally high $CO_2/CH_4$ selectivity, *J. Am. Chem. Soc.*, 140 (32), 10113–10116.

[14] Flaig, R.W., Osborn Popp, T.M., Fracaroli, A.M., Kapustin, E.A., Kalmutzki, M.J., Altamimi, R.M., Fathieh, F., Reimer, J.A., and Yaghi, O.M., 2017, The chemistry of $CO_2$ capture in an amine-functionalized metal-organic framework under dry and humid conditions, *J. Am. Chem. Soc.*, 139 (35), 12125–12128.

[15] Marti, A.M., Venna, S.R., Roth, E.A., Culp, J.T., and Hopkinson, D.P., 2018, Simple fabrication method for mixed matrix membranes with in situ MOF growth for gas separation, *ACS Appl. Mater. Interfaces*, 10 (29), 24784–24790.

[16] Zhang, S., Zhang, J., Zhang, Y., and Deng, Y., 2017, Nanoconfined ionic liquids, *Chem. Rev.*, 117 (10), 6755–6833.

[17] Zeng, S., Zhang, X., Bai, L., Zhang, X., Wang, H., Wang, J., Bao, D., Li, M., Liu, X., and Zhang, S., 2017, Ionic-liquid-based $CO_2$ capture systems: Structure, interaction and process, *Chem. Rev.*, 117 (14), 9625–9673.

[18] Kinik, F.P., Altintas, C., Balci, V., Koyuturk, B., Uzun, A., and Keskin, S., 2016, [BMIM][$PF_6$] Incorporation doubles $CO_2$ selectivity of ZIF-8: Elucidation of interactions and their consequences on performance, *ACS Appl. Mater. Interfaces*, 8 (45), 30992–31005.

[19] Oliveira, L.T., Gonçalves, R.V., Gonçalves, D.V., de Azevedo, D.C.S., and de Lucena, S.M.P., 2019, Superior performance of mesoporous MOF MIL-100 (Fe) impregnated with ionic liquids for $CO_2$ adsorption, *J. Chem. Eng. Data*, 64 (5), 2221–2228.

[20] Cavka, J.H., Jakobsen, S., Olsbye, U., Guillou, N., Lamberti, C., Bordiga, S., and Lillerud, K.P., 2008, A new zirconium inorganic building brick forming metal organic frameworks with exceptional stability, *J. Am. Chem. Soc.*, 130 (42), 13850–13851.

[21] Pirzadeh, K., Esfandiari, K., Ghoreyshi, A.A., and Rahimnejad, M., 2020, $CO_2$ and $N_2$ adsorption and separation using aminated UiO-66 and $Cu_3(BTC)_2$: A comparative study, *Korean J. Chem. Eng.*, 37 (3), 513–524.

[22] Sun, Y., Huang, H., Vardhan, H., Aguila, B., Zhong, C., Perman, J.A., Al-Enizi, A.M., Nafady, A., and Ma, S., 2018, Facile approach to graft ionic liquid into MOF for improving the efficiency of $CO_2$ chemical fixation, *ACS Appl. Mater. Interfaces*, 10 (32), 27124–27130.

[23] Øien, S., Wragg, D., Reinsch, H., Svelle, S., Bordiga, S., Lamberti, C., and Lillerud, K.P., 2014, Detailed structure analysis of atomic positions and defects in zirconium metal-organic frameworks, *Cryst. Growth Des.*, 14 (11), 5370–5372.

[24] Sezginel, K.B., Keskin, S., and Uzun, A., 2016, Tuning the gas separation performance of CuBTC

by ionic liquid incorporation, *Langmuir*, 32 (4), 1139–1147.

[25] Durak, Ö., Kulak, H., Kavak, S., Polat, H.M., Keskin, S., and Uzun, A., 2020, Towards complete elucidation of structural factors controlling thermal stability of IL/MOF composites: Effects of ligand functionalization on MOFs, *J. Phys.: Condens. Matter*, 32 (48), 484001.

[26] Kavak, S., Kulak, H., Polat, H.M., Keskin, S., and Uzun, A., 2020, Fast and selective adsorption of methylene blue from water using [BMIM][$PF_6$]-incorporated UiO-66 and $NH_2$-UiO-66, *Cryst. Growth Des.*, 20 (6), 3590–3595.

[27] Huddleston, J.G., Visser, A.E., Reichert, W.M., Willauer, H.D., Broker, G.A., and Rogers, R.D., 2001, Characterization and comparison of hydrophilic and hydrophobic room temperature ionic liquids incorporating the imidazolium cation, *Green Chem.*, 3 (4), 156–164.

[28] Ferreira, T.J., Ribeiro, R.P.P.L., Mota, J.P.B., Rebelo, L.P.N., Esperança, J.M.S.S., and Esteves, I.A.A.C., 2019, Ionic liquid-impregnated metal-organic frameworks for $CO_2/CH_4$ separation, *ACS Appl. Nano Mater.*, 2 (12), 7933–7950.

[29] Arrozi, U.S.F., Wijaya, H.W., Patah, A., and Permana, Y., 2015, Efficient acetalization of benzaldehydes using UiO-66 and UiO-67: Substrates accessibility or Lewis acidity of zirconium, *Appl. Catal., A*, 506, 77–84.

[30] Kim, H.K., Yun, W.S., Kim, M.B., Kim, J.Y., Bae, Y.S., Lee, J.D., and Jeong, N.C., 2015, A chemical route to activation of open metal sites in the copper-based metal-organic framework materials HKUST-1 and Cu-MOF-2, *J. Am. Chem. Soc.*, 137 (31), 10009–10015.

[31] Vicent-Luna, J.M., Gutiérrez-Sevillano, J.J., Anta, J.A., and Calero, S., 2013, Effect of room-temperature ionic liquids on $CO_2$ separation by a Cu-BTC metal-organic framework, *J. Phys. Chem. C*, 117 (40), 20762–20768.

[32] Xia, X., Hu, G., Li, W., and Li, S., 2019, Understanding reduced $CO_2$ uptake of ionic liquid/metal–organic framework (IL/MOF) composites, *ACS Appl. Nano Mater.*, 2 (9), 6022–6029.

[33] Aki, S.N.V.K., Mellein, B.R., Saurer, E.M., and Brennecke, J.F., 2004, High-pressure phase behavior of carbon dioxide with imidazolium-based ionic liquids, *J. Phys. Chem. B*, 108 (52), 20355–20365.

[34] Muldoon, M.J., Aki, S.N.V.K., Anderson, J.L., Dixon, J.K., and Brennecke, J.F., 2007, Improving carbon dioxide solubility in ionic liquids, *J. Phys. Chem. B*, 111 (30), 9001–9009.

[35] Kazemiabnavi, S., Zhang, Z., Thornton, K., and Banerjee, S., 2016, Electrochemical stability window of imidazolium-based ionic liquids as electrolytes for lithium batteries, *J. Phys. Chem. B*, 120 (25), 5691–5702.